Compact Substrate Integrated Waveguide Quasi-End-Fire Antenna for CubeSat Integration

Compact Substrate Integrated Waveguide Quasi-End-Fire Antenna for CubeSat Integration

Khalid M. Alrushud, *Student Member, IEEE*, Victoria Gómez-Guillamón Buendía, *Member, IEEE*, Symon K. Podilchak, *Member, IEEE*

***Abstract*—A planar quasi-end-fire surface wave antenna using substrate integrated waveguide (SIW) technology for integration with CubeSats and other small satellites is proposed in this letter. This antenna can be attached to the body of the satellite, resulting in a compact and low-cost design. A quasi-end-fire beam pattern is achieved by the radiation of the fundamental TM_0 surface wave mode at the edge of a grounded dielectric slab (GDS). This mode is excited by a leaky SIW T-junction creating a uniform wavefront that propagates through a truncated parallel-plate waveguide (PPW). A matching section based on an array of sub-wavelength patches is also added at the interface between the PPW and the GDS for reduced reflections and improved antenna radiation performance. The measured prototype demonstrated realized gain values of 13.3 dBi at 18.6 GHz for a competitive structure size of $5\lambda_0 \times 4.8\ \lambda_0$ and with a simulated total radiation efficiency of 93.4%, providing high data rate capabilities for downlink communications. This antenna could be suitable for CubeSat or other small satellite commercial missions, for example, Earth and planetary observations or inter-satellite links.**

***Index Terms*—Substrate integrated waveguide, leaky waves, CubeSats, end-fire, surface waves, surface-wave antenna.**

I. Introduction

As a result of the increasing interest for affordable Earth and planetary observation networks, telemetry systems, tracking and control, as well as remote sensing and navigation services, small satellites have seen a rapid growth in the last two decades. Due to this technology trend, and whilst conventional satellite systems cannot be entirely replaced by small satellites, many academic and industrial efforts are focusing on the development of compact and innovative systems. Subsequently, the trend for these small satellites is to offer more communication services in a generally highly constrained volume when compared to larger satellites. This is especially challenging for antenna engineers as additionally to the RF performance requirements, they also need to consider the inherent CubeSat constraints in terms of volume, weight and cost [1], [2].

Following these trends, there are challenging requirements and antenna specifications in terms of pattern directivity and realized gain, for example, that could restrict design selection when considering said high data rate applications. This has resulted in extensive research into CubeSat antennas which have focused on achieving these important requirements. For instance, the work reported by NASA for remote sensing, which integrated large antennas with a compact stowage box whilst aiming for high directivity, was based on a meshed deployable reflector antenna system having a stowed volume of 3U [3], [4]. Additionally, in [5], a folded panel reflectarray operating at X-band was stowed in a 6U CubeSat providing a lightweight configuration (<1 kg) whilst keeping high gain values around 29.2 dBi. Planar and non-deployable structures have also been explored when lower gains are required, for instance, as with the folded-shorted patch compact array for telemetry and inter-satellite links [6]–[8]. These miniaturized patch antennas usually have a resonant length of $\lambda/2$, and can be reduced to a fraction of $\lambda/4$ by a shorting wall and structure folding. These antennas have been designed at UHF and L-band frequencies for small satellites [9] such as the Maritime Monitoring and Messaging Microsatellite (M3MSat) mission for the Canadian Space Agency (CSA).

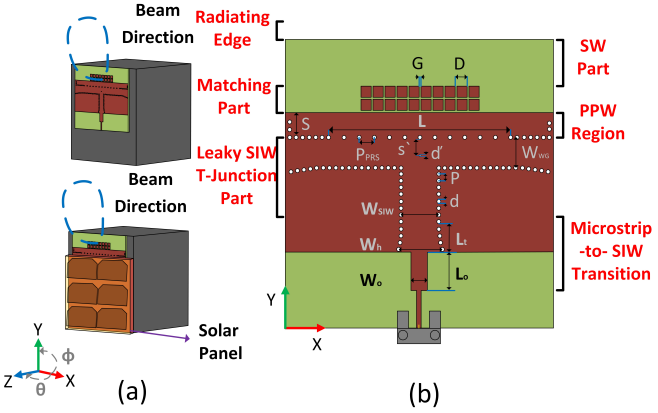

Fig. 1. (a) Examples of the placement of the proposed antenna on a 1U CubeSat illustrating the quasi-end-fire beam pattern, (b) top-view of the proposed end-fire antenna structure defining the design parameters and sections. As illustrated in (a), a solar panel array could also be placed on top of the planar antenna if the microstrip-substrate integrated waveguide (SIW) feedline is removed and the structure is excited by a vertical probe. This is possible because the covered part of the SWA would all be metal.

Planar antennas attached to the satellite, as proposed herein (see Fig. 1), could then be advantageous with respect to deployable systems, due to the degrees of freedom when adopting PCB design and possibly higher reliability in space environments, where debris and strong vibrations or extreme thermal conditions during launching could lead to failed deployments [1], [2], [10]. Moreover, they also allow for innovative integration techniques such as on top of solar cells, as presented in [11]–[13]. In this way, extra space is made available on the satellite for additional antennas, sensors, image capturing devices, etc. as well as more solar cells.

Many of these CubeSat antenna examples offer broadside radiation. However, due to the limited space available, chassis placement, and the satellite structure integration requirements,

Manuscript received X X, 2021. K. Alrushud and S.K. Podilchak are with the School of Engineering, Institute for Digital Communications, The University of Edinburgh, Edinburgh, Scotland, UK (e-mail: s.podilchak@ed.ac.uk).

K. Alrushud is also with King Abdulaziz City for Science and Technology (KACST), Riyadh, Saudi Arabia (e-mail: kalrushud@kacst.edu.sa).

V. G. Buendia is with the Radar Technology Department, TNO, The Hague, The Netherlands (e-mail: victoria.gomez@tno.nl).

Work was supported by King Abdulaziz City for Science and Technology.

This letter has supplementary downloadable material available at https://ieeexplore.ieee.org, as provided by the authors.

the beam pattern of the antenna may be pointing in the wrong direction. Therefore, it may be necessary to steer the antenna radiation in a different direction such as end-fire, being useful for downlink communications for instance. Also, there are not many examples in the literature of planar end-fire antennas specifically designed for CubeSat applications, and this may be due integration constraints when aiming to achieve proper end-fire or quasi-end-fire radiation. More classical implementations, such as Yagi-Uda arrays [14] or complementary dipoles [15], may not be suitable if metallic structures are underneath the radiating element or the space available is highly constrained. These challenges require more clever solutions such as miniaturization [16] or mechanical steering of the antenna [17].

We propose herein a compact planar K-band end-fire antenna (see Fig. 1) based on substrate integrated waveguide (SIW) technology [18], [19], leaky wave (LW) principles, and transverse magnetic (TM) surface waves (SWs). The newly studied antenna design employes an adapted version of the parallel-plate waveguide (PPW) launcher (i.e. a non-radiating feed system), as previously reported for a lower frequency band in [20], [21]. Both of those works focused on the implementation and optimization of the PPW launcher as a feeding network suitable for slotted PPW antenna arrays [20], and, a phase control technique to help achieve a uniform and guided wavefront for a non-radiating, 2-port demonstrator [21]. The excitation efficiency, which was more than 90% in those previous works, as well as the controlled phase front demonstrated, inspired the modification and adaptation of this feed system to drive a new end-fire antenna suitable for downlink applications at K-band on CubeSats and where directive beam patterns are required. The thickness of the substrate was also increased from [20], [21], mainly, to improve and further enhance the SW excitation efficiency for the designed and experimentally measured surface-wave antenna (SWA), providing alternatives to other SW feeding schemes as in [22] and references therein.

Detailed simulations, numerical analysis, and measurements examining the performance of the SWA are reported in this letter. This proposed planar structure could also be attached to the body of the satellite, achieving a compact and low-profile design. Figure 1(a) illustrates examples of the possible CubeSat placement as well as its far-field beam pattern. An overview on the antenna design is provided in Section II. Discussions on the simulated and measured results will follow in Section III while conclusions are drawn in Section IV.

II. Antenna Design Approach

The proposed end-fire antenna consists of four parts: the microstrip to SIW transition, the leaky SIW T-junction using a PPW, the matching section made by a subwavelength array of patches, and the grounded dielectric slab (GDS) section for bound SW propagation and then radiation (see Fig. 1(b)).

A. Leaky SIW T-Junction

The implementation of the conventional T-junction based on SIW technology is the first step in the design process [18], [19]. The primary function of this T-junction is to divide the power over the aperture equally. It should be mentioned that adding an extra inductive post in the middle of this junction will improve the matching [23]. This inductive via has been optimised with a diameter of $d' = 0.21\,\text{mm}$ and a position $S' = 3.07\,\text{mm}$ (see Fig. 1 (b)).

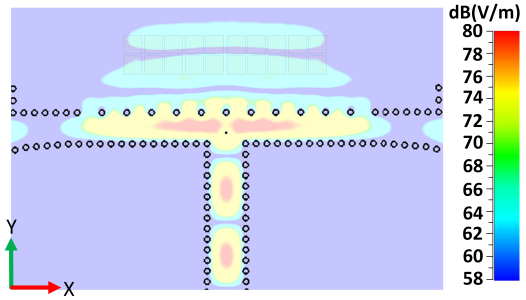

Fig. 2. Simulated electric-field showing a uniform distribution within the PPW, the matching section, and the GDS.

The SIW TE_{10} fundamental mode is coupled into the transverse electromagnetic (TEM) mode of the PPW section. This is made possible since the broad arms of the T-junction walls are made lossy to leak out power [21], [24]. Thus vias are required to be separated more than the regular condition for guided and confined propagation within the SIW ($P \leq 2d$, where P and d are the via periodicity and diameter, respectively [18], [25]). This creates a partially reflective screen (PRS) to allow leakage from the SIW structure to the PPW. The complex propagation constant ($\gamma = \alpha + j\beta$) for the relevant LW mode needs to be analyzed to design this PRS, where α and β are the attenuation and phase constants, respectively. Moreover, α depends on the spacing between the vias, and the higher this spacing the shorter this PRS length L needs to be [21], [26]. Furthermore, α needs to be high enough for suitable leakage; i.e. such that most of the power from the input feed point is coupled into the PPW section, and not reaching the two side arm ends of the SIW T-junction.

To achieve uniform phase propagation inside the PPW region and the matching section (see Fig. 2), the operating frequency must be slightly above the cutoff frequency of the SIW, which in this case has been selected to be 18 GHz, and, at the splitting condition where $\beta \approx \alpha$ [24]. The PRS aperture length L can then be found by setting the aperture efficiency to 90%, requiring $L = 2.3/\alpha$ [24].The dispersive analysis depending on the antenna parameters can then be performed by a transverse equivalent network (TEN) [27], which is based on an equivalent transmission line circuit of the structure to define the impedance transverse resonance equation related to the complex propagation constant. The adopted TEN circuit is the same as in [21] and is depicted in Fig. 3, where the dispersive analysis results are also included. It can be observed that the splitting condition occurs in the proximity of 18 GHz.

Following these preliminary numerical calculations as an initial step, all structure parameters were optimized further using CST Microwave Studio, and the values for this leaky T-Junction are: $W_{SIW} = 6.99\,\text{mm}$, $d = 1\,\text{mm}$, $P = 1.93\,\text{mm}$, $W_{WG} = 5.67\,\text{mm}$, $P_{PRS} = 4.5\,\text{mm}$, and $L = 54\,\text{mm}$. Figure 1 (b) displays these parameters and their position within

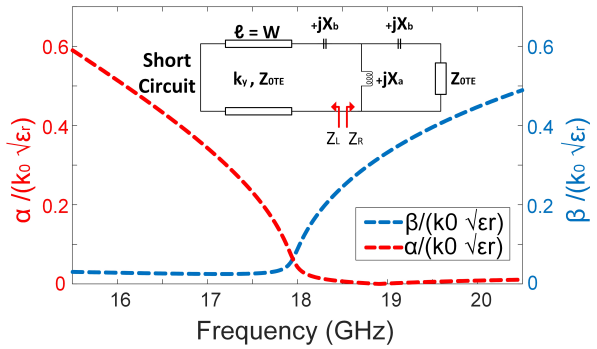

Fig. 3. TEN circuit model and the normalized LW phase and attenuation constants. The splitting-condition; i.e. $\alpha \approx \beta$ can be observed at ≈18 GHz.

the designed structure considering ROGERS RT5880 as the employed substrate with a relative permittivity of ϵ_r = 2.2 and a thickness of 1.575 mm.

B. Matching Section and Grounded Dielectric Slab

The distance to the truncation of the PPW region is defined as $S = 5.33$ mm (see Fig. 1 (b)), this is because it is required to be set as a multiple of $\lambda_g/4$, being λ_g the guided wavelength. This can reduce any reflected power from the leaky T-Junction, and by following conventional $\lambda_g/4$ transformer concepts to control impedances [27]. The same applies to the matching section, defined by sub-wavelength patches, which is essential to prevent an abrupt transition from the TEM mode inside the PPW to the TM_0 SW mode of the GDS.

The number of these patches also helps to control the leaked power from the T-junction allowing for a smooth transition (see Fig. 2). During the simulations and optimizations in CST it was found that the number of sub-wavelength patches for this SWA should be 10 for every row. Otherwise, by the addition of more patches, an unwanted increase of the side lobe levels can be observed in the far-field, similarly if no matching section was present (all results not shown due to brevity).

The surface grid impedance Z_g is also related to G, the gap between the patches [28], and allows the fields within the matching section to be controlled and well-matched to the TM_0 SW mode of the GDS. After following the equations in [28], the microstrip patch size was set to $D = 3.485$ mm with $G = 0.355$ mm. Also, as it is well known for travelling wave antennas [29], reflections need to be minimized to prevent unwanted backward radiation, therefore matching techniques, such as the $\lambda_g/4$ PPW section and the sub-wavelength array of patches, are needed to improve the front-to-back ratio. This is examined in Fig. 4 where it can be observed that the backward radiation is considerably higher, by more than 12 dB, when the patches are removed. This is also the case for the GDS section (see Fig. 1 (b)), as it is important to optimize its length and to prevent reflections back from the truncated edge of the dielectric.

At this point within the feed structure and after the sub-wavelength matching section, the phase propagation constant is already demonstrating slow-wave behaviour (not fully discussed for brevity), and therefore, the TM_0 SW within the GDS section can be radiated at structure discontinuity. This achieves end-fire radiation defining the SWA, and this distance was optimised after some further CST simulations to be 8 mm. It should also be mentioned that this SWA was designed in the presence of a ground plane, and when attached to the CubeSat body, the far-field beam pattern can deviate from full-end-fire towards quasi-end-fire. However, the structure can also be modified and optimised to remove the ground plane of the GDS making it a full-end-fire SWA useful for other applications as not to be placed on a metallic surface.

C. Microstrip to SIW Transition

The tapered microstrip line [30] is widely used for the microstrip-to-SIW transitions as it enhances the matching from the 50-Ω microstrip line to the SIW input [30]–[32]. However, there are cases in which the impedance of the SIW section is higher than the one in the microstrip line, and therefore, conventional microstrip tappering cannot be implemented. This occurs in our structure and this is solved by tappering the SIW instead [32]. The parameters for this section have been optimized as: $W_h = 9$ mm, $L_t = 8.85$ mm, $W_o = 4.85$ mm, and $L_o = 12.2$ mm.

III. Simulations and Measurements

The quasi-end-fire SWA was fabricated and measured in a calibrated anechoic chamber. Results are reported in Figs. 4-8. Agreement was also generally observed between the simulations and measurements.

A minor frequency shift can be noted for the reflection coefficient in Fig. 5, which is likely related to possible manufacturing tolerances, including via drilling, metallization, and substrate property variation. To understand this frequency shift further, additional simulations were performed for different relative permittivities. After this parametric analysis, results suggested that $\epsilon_r \approx 2$, is more representative of the substrate at about 18 GHz (rather than ϵ_r = 2.2 as rated on the data sheet). This effect is also shown in Fig. 6 where there is a better agreement between the simulated and measured realised gain versus frequency. This noted frequency shift in $|S_{11}|$ and the realized gain is likely related anisotropy of the GDS where the relative dielectric constant in the vertical direction can be different than the horizontal direction at higher frequencies [33]–[35]. This anisotropy, which can be significant for thick substrates, is a result of manufacturing and has some frequency dependence (see [35] pp. 758, Appendix A). As discussed in [33], by changing the value for the dielectric constant (a similar procedure was reported in [22]), a better agreement between simulations and the measurements can be observed.

When the SWA is attached to the satellite body, there is little effect on its performance as observed in the dashed lines of Fig. 5 due to the presence of a large ground plane. Also, the measurements imply that the centre frequency for the quasi-end-fire SWA is higher than originally intended. In fact, results depicted in Fig. 5 show that the centre frequency for the fabricated structure was around 18.6 GHz and not 18.1 GHz as per the original design. This can be observed by checking the measured $|S_{11}|$, which is below -15 dB at around 18.6 GHz.

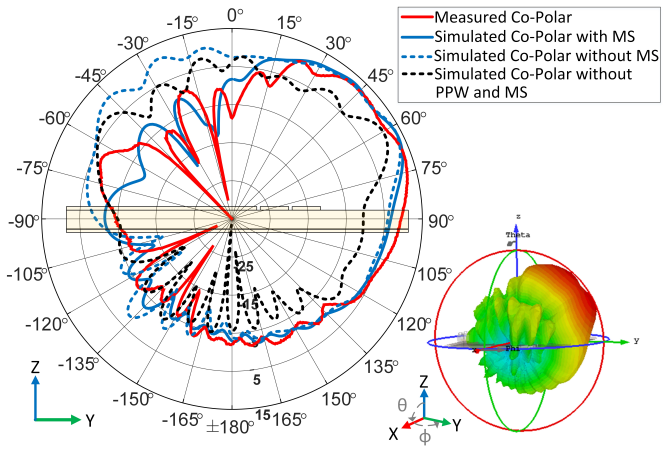

Fig. 4. Simulated and measured beam patterns in the y-z plane ($\phi = 90°$). Measured results are plotted at 18.6 GHz. Dashed lines represent the simulated beam patterns without the matching section (MS) and without the PPW and MS. The simulated 3D pattern is also reported (right).

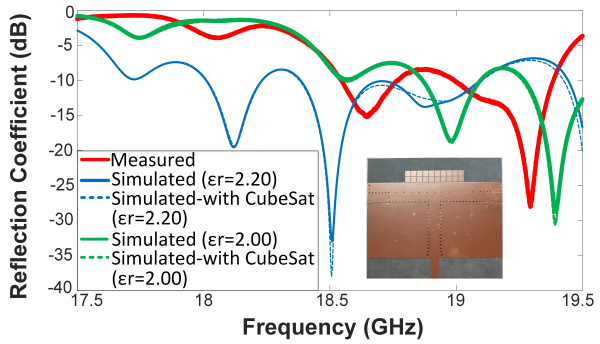

Fig. 5. Reflection coefficient versus frequency for the designed SWA (see inset). It should be pointed out that initial simulations were completed considering $\epsilon_r = 2.2$ (blue solid line) while the green lines consider practical permittivity tolerances. Simulations on the CubeSat body are also reported.

Simulation and measurement results for the far-field beam patterns are shown in Figs. 4 and 7. The maximum measured realized gain is 13.3 dBi at 18.6 GHz (due to the shifted frequency of operation) in the y-z plane ($\phi = 90°$) (see Fig. 4), which is slightly reduced in comparison to the simulated 14 dBi. This gain reduction is likely related to the noted practical change in the ϵ_r value and to the employed connector. Also, the simulated radiation efficiency is over 92% with and without the connector from 18 GHz up to 18.8 GHz. However, the total efficiency is between 84% and 95% for the antenna without the connector and between 75% to 94% with the connector for the same frequency range.

The measured realized gain in the x-y plane ($\theta = 90°$) (see Fig. 7) is 5.5 dBi. This value is significantly lower because the main beam is pointing towards quasi-end-fire ($\theta = 70°$) and not full end-fire ($\theta = 90°$). Regardless of the practicalities mentioned above, general agreement between the simulated

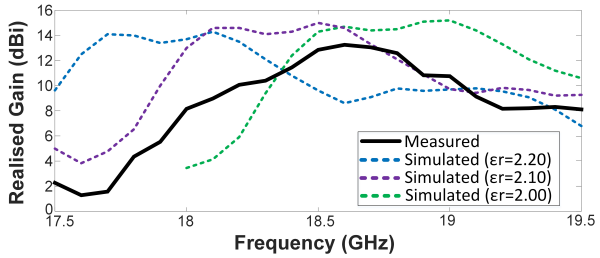

Fig. 6. Measured and simulated maximum realised gain in the y-z plane.

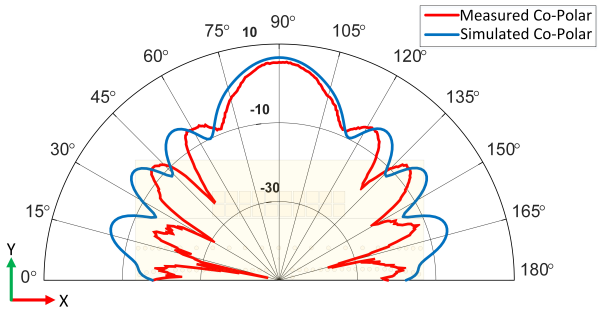

Fig. 7. Simulated and measured beam patterns in the x-y plane ($\theta = 90°$).

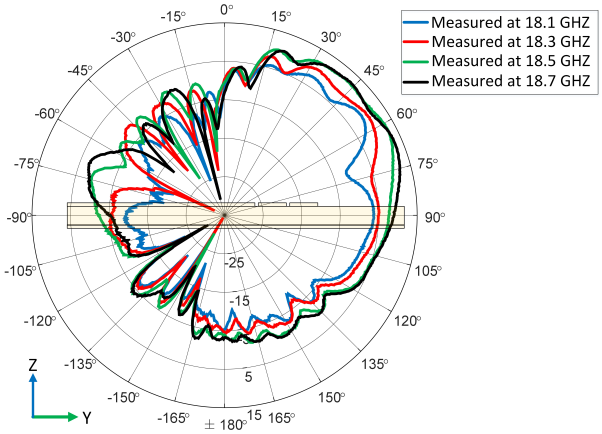

Fig. 8. Measured beam patterns for different frequencies from 18.1 to 18.7 GHz in the y-z plane ($\phi = 90°$).

and measured beam patterns can be observed. Figure 8 also reports the measured beam patterns for the the y-z plane ($\phi = 90°$) over a wide frequency range from 18.1 GHz up to 18.7 GHz. It can be observed that the pointing angles and sidelobe levels are very similar through frequency. These features can support high data-rate downlink communications. Also, as compared to other antennas in the literature [36]–[41], our proposed SWA offers a very competitive high radiation efficiency whilst maintaining a compact structure size. This is outlined in Tab. I of the supplementary material for this paper.

IV. Conclusion

A planar quasi-end-fire surface wave antenna has been introduced in this letter for end-fire operation at K-band. The structure has been designed using SIW technology for integration on CubeSats and other small satellites. This quasi-end-fire performance has been achieved by edge radiation of the fundamental TM_0 SW mode from a GDS. This mode was efficiently excited by a leaky SIW T-junction which created a uniform wavefront that propagates through a truncated PPW. A matching section was also included which was based on an array of sub-wavelength patches placed at the interface between the PPW and the GDS for a smooth transition and reduced structure reflections. The fabricated SWA obtained a realized gain of 13.3 dBi, demonstrating also good agreement between the simulated and measured beam patterns.

Acknowledgement

The Authors would like to thank José Luis Gómez Tornero, George Goussetis, Davide Comite, Paolo Baccarelli and Paolo Burghignoli for their contributions to the previous and related structures found in [20], [21]. The Authors would also like to acknowledge Maksim Kuznetcov, Zain Shafiq and Callum Hodgkinson for their assistance during measurements.

REFERENCES

[1] S. Gao, Y. Rahmat-Samii, R. E. Hodges, and X.-X. Yang, "Advanced antennas for small satellites," *Proceedings of the IEEE*, vol. 106, no. 3, pp. 391–403, 2018.

[2] Y. Rahmat-Samii, V. Manohar, and J. M. Kovitz, "For satellites, think small, dream big: A review of recent antenna developments for cubesats." *IEEE Antennas and Propagation Magazine*, vol. 59, no. 2, pp. 22–30, 2017.

[3] Y. Rahmat-Samii, V. Manohar, J. M. Kovitz, R. E. Hodges, G. Freebury, and E. Peral, "Development of highly constrained 1 m ka-band mesh deployable offset reflector antenna for next generation cubesat radars," *IEEE Transactions on Antennas and Propagation*, vol. 67, no. 10, pp. 6254–6266, 2019.

[4] N. Chahat, J. Sauder, M. Mitchell, N. Beidleman, and G. Freebury, "One-meter deployable mesh reflector for deep-space network telecommunication at X-band and Ka-band," *IEEE Transactions on Antennas and Propagation*, vol. 68, no. 2, pp. 727–735, 2019.

[5] R. E. Hodges, N. Chahat, D. J. Hoppe, and J. D. Vacchione, "A deployable high-gain antenna bound for mars: Developing a new folded-panel reflectarray for the first cubesat mission to mars." *IEEE Antennas and Propagation Magazine*, vol. 59, no. 2, pp. 39–49, 2017.

[6] Y. Li, S. K. Podilchak, D. E. Anagnostou, C. Constantinides, and T. Walkinshaw, "Compact antenna for picosatellites using a meandered folded-shorted patch array," *IEEE Antennas and Wireless Propagation Letters*, vol. 19, no. 3, pp. 477–481, 2020.

[7] S. K. Podilchak, A. P. Murdoch, and Y. M. M. Antar, "Compact, microstrip-based folded-shorted patches: PCB antennas for use on microsatellites," *IEEE Antennas and Propagation Magazine*, vol. 59, no. 2, pp. 88–95, 2017.

[8] S. K. Podilchak, M. Caillet, D. Lee, Y. M. M. Antar, L. C. Chu, J. Cain, M. Hammar, D. Caldwell, and E. Barron, "A compact circularly polarized antenna using an array of folded-shorted patches," *IEEE Transactions on Antennas and Propagation*, vol. 61, no. 9, pp. 4861–4867, 2013.

[9] "Maritime monitoring and messaging microsatellite (M3MSat) mission," https://www.asc-csa.gc.ca/eng/satellites/m3msat/default.asp, accessed: 2021-03-20.

[10] N. E. Chahat, "A mighty antenna from a tiny cubesat grows," *IEEE Spectrum*, vol. 55, no. 2, pp. 32–37, 2018.

[11] S. K. Podilchak, D. Comite, B. K. Montgomery, Y. Li, V. G.-G. Buendía, and Y. M. M. Antar, "Solar-panel integrated circularly polarized meshed patch for cubesats and other small satellites," *IEEE Access*, vol. 7, pp. 96 560–96 566, 2019.

[12] T. Yekan and R. Baktur, "Conformal integrated solar panel antennas: Two effective integration methods of antennas with solar cells." *IEEE Antennas and Propagation Magazine*, vol. 59, no. 2, pp. 69–78, 2017.

[13] S. Zarbakhsh, M. Akbari, M. Farahani, A. Ghayekhloo, T. A. Denidni, and A.-R. Sebak, "Optically transparent subarray antenna based on solar panel for cubesat application," *IEEE Transactions on Antennas and Propagation*, vol. 68, no. 1, pp. 319–328, 2019.

[14] J. Huang and A. Densmore, "Microstrip yagi array antenna for mobile satellite vehicle application," *IEEE Transactions on Antennas and Propagation*, vol. 39, no. 7, pp. 1024–1030, 1991.

[15] W.-J. Lu, J.-W. Shi, K.-F. Tong, and H.-B. Zhu, "Planar endfire circularly polarized antenna using combined magnetic dipoles," *IEEE Antennas and Wireless Propagation Letters*, vol. 14, pp. 1263–1266, 2015.

[16] V. Gómez-Guillamón Buendía, S. K. Podilchak, S. Liberto, D. E. Anagnostou, G. Goussetis, C. Constantinides, T. Walkinshaw, and M. van der Vorst, "Compact end-fire antenna designs for picosat integration and other small satellite missions," in *2020 50th European Microwave Conference (EuMC)*, 2021, pp. 463–466.

[17] S. Liu, R. Raad, P. I. Theoharis, and F. E. Tubbal, "A printed yagi antenna for cubesat with multi-frequency tilt operation," *Electronics*, vol. 9, no. 6, 2020.

[18] D. Deslandes and K. Wu, "Single-substrate integration technique of planar circuits and waveguide filters," *IEEE Transactions on microwave theory and Techniques*, vol. 51, no. 2, pp. 593–596, 2003.

[19] K. Wu, M. Bozzi, and N. J. Fonseca, "Substrate integrated transmission lines: Review and applications," *IEEE Journal of Microwaves*, vol. 1, no. 1, pp. 345–363, 2021.

[20] V. G.-G. Buendia, S. K. Podilchak, G. Goussetis, and J.-L. Gomez-Tornero, "A TM_0 surface wave launcher by microstrip and substrate integrated waveguide technology," in *2017 11th European Conference on Antennas and Propagation (EUCAP)*. IEEE, 2017, pp. 3859–3862.

[21] V. G.-G. Buendía, S. K. Podilchak, D. Comite, P. Baccarelli, P. Burghignoli, J. L. G. Tornero, and G. Goussetis, "Compact leaky SIW feeder offering tem parallel plate waveguide launching," *IEEE Access*, vol. 7, pp. 13 373–13 382, 2019.

[22] S. K. Podilchak, P. Baccarelli, P. Burghignoli, A. P. Freundorfer, and Y. M. M. Antar, "Analysis and design of annular microstrip-based planar periodic leaky-wave antennas," *IEEE Transactions on Antennas and Propagation*, vol. 62, no. 6, pp. 2978–2991, 2014.

[23] S. Germain, D. Deslandes, and K. Wu, "Development of substrate integrated waveguide power dividers," in *CCECE 2003-Canadian Conference on Electrical and Computer Engineering. Toward a Caring and Humane Technology*, vol. 3. IEEE, 2003, pp. 1921–1924.

[24] J. L. G. Tornero, A. M. Ros, M. A. Martinez, A. M. Sala, G. Goussetis, and S. K. Podilchak, "A simple parallel-plate wave launcher in substrate integrated waveguide technology," in *2015 IEEE International Symposium on Antennas and Propagation & USNC/URSI National Radio Science Meeting*. IEEE, 2015, pp. 480–481.

[25] F. Xu and K. Wu, "Guided-wave and leakage characteristics of substrate integrated waveguide," *IEEE Transactions on Microwave Theory and Techniques*, vol. 53, no. 1, pp. 66–73, 2005.

[26] P. Burghignoli, G. Lovat, and D. R. Jackson, "Analysis and optimization of leaky-wave radiation at broadside from a class of 1-D periodic structures," *IEEE Transactions on Antennas and Propagation*, vol. 54, no. 9, pp. 2593–2604, 2006.

[27] D. Pozar, "Microwave Engineering, 4th Edition, John Wiley & Sons," 2012.

[28] O. Luukkonen, C. Simovski, G. Granet, G. Goussetis, D. Lioubtchenko, A. V. Raisanen, and S. A. Tretyakov, "Simple and accurate analytical model of planar grids and high-impedance surfaces comprising metal strips or patches," *IEEE Transactions on Antennas and Propagation*, vol. 56, no. 6, pp. 1624–1632, 2008.

[29] F. J. Zucker and R. C. Johnson, "Surface-wave antennas," *Antenna Engineering Handbook*, vol. 4, 2007.

[30] D. Deslandes, "Design equations for tapered microstrip-to-substrate integrated waveguide transitions," in *2010 IEEE MTT-S International Microwave Symposium*. IEEE, 2010, pp. 704–707.

[31] D. Deslandes and K. Wu, "Integrated microstrip and rectangular waveguide in planar form," *IEEE microwave and wireless components letters*, vol. 11, no. 2, pp. 68–70, 2001.

[32] E. D. Caballero, A. B. Martinez, H. E. Gonzalez, O. M. Belda, and V. B. Esbert, "A novel transition from microstrip to a substrate integrated waveguide with higher characteristic impedance," in *2013 IEEE MTT-S International Microwave Symposium Digest (MTT)*. IEEE, 2013, pp. 1–4.

[33] N. Alexopoulos, "Integrated-circuit structures on anisotropic substrates," *IEEE Transactions on Microwave Theory and Techniques*, vol. 33, no. 10, pp. 847–881, 1985.

[34] D. Pozar, "Radiation and scattering from a microstrip patch on a uniaxial substrate," *IEEE Transactions on Antennas and Propagation*, vol. 35, pp. 613–621, 1987.

[35] R. Garg, P. Bhartia, and A. Ittipiboon, "Microstrip antenna design handbook," 2000.

[36] M. M. S. Taheri, A. Abdipour, S. Zhang, and G. F. Pedersen, "Integrated millimeter-wave wideband end-fire 5g beam steerable array and low-frequency 4g lte antenna in mobile terminals," *IEEE Transactions on Vehicular Technology*, vol. 68, no. 4, pp. 4042–4046, 2019.

[37] P. Wang, Q. Wu, R.-B. He, and Y. Shao, "Design of low profile and wideband end-fire antenna using metasurface," *IEEE Access*, vol. 8, pp. 35 752–35 758, 2020.

[38] J. Zhang, K. Zhao, L. Wang, S. Zhang, and G. F. Pedersen, "Dual-polarized phased array with end-fire radiation for 5g handset applications," *IEEE Transactions on Antennas and Propagation*, vol. 68, no. 4, pp. 3277–3282, 2019.

[39] A. Li and K.-M. Luk, "Millimeter-wave end-fire magneto-electric dipole antenna and arrays with asymmetrical substrate integrated coaxial line feed," *IEEE Open Journal of Antennas and Propagation*, vol. 2, pp. 62–71, 2020.

[40] A. A. Omar, J. Park, W. Kwon, and W. Hong, "A compact wideband vertically polarized end-fire millimeter-wave antenna utilizing slot, dielectric, and cavity resonators," *IEEE Transactions on Antennas and Propagation*, 2021.

[41] N. O. Parchin, J. Zhang, R. A. Abd-Alhameed, G. F. Pedersen, and S. Zhang, "A planar dual-polarized phased array with broad bandwidth and quasi end-fire radiation for 5g mobile handsets," *IEEE Transactions on Antennas and Propagation*, 2021.